### Magnetic vortex control with current-induced axial magnetization in centrosymmetric Weyl materials 🕗

Special Collection: Topological and Chiral Matter - Physics and Applications

J. G. Yang 💿 ; Yaroslav Tserkovnyak 💿 ; D. A. Pesin 🗷 💿



Appl. Phys. Lett. 124, 203102 (2024) https://doi.org/10.1063/5.0202451

A CHORUS





#### Articles You May Be Interested In

Intrinsic insulating transport characteristics in low-carrier density EuCd<sub>2</sub>As<sub>2</sub> films

Appl. Phys. Lett. (January 2024)

Prediction of ferromagnetic Weyl semimetal and antiferromagnetic topological insulator phases in MnHg<sub>2</sub>Te<sub>3</sub>

Appl. Phys. Lett. (November 2022)

Weyl nodes and hybrid nodal loop with spin-orbit coupling in  $\mathrm{W}_2\mathrm{TeSe}$ 

Appl. Phys. Lett. (November 2023)

Webinar From Noise to Knowledge Zurich Universität Konstanz



# 28 April 2025 17:29:55

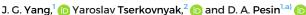
## Magnetic vortex control with current-induced axial magnetization in centrosymmetric Weyl materials

Cite as: Appl. Phys. Lett. 124, 203102 (2024); doi: 10.1063/5.0202451 Submitted: 4 February 2024 · Accepted: 9 May 2024 · Published Online: 15 May 2024













#### **AFFILIATIONS**

<sup>1</sup>Department of Physics, University of Virginia, Charlottesville, Virginia 22904, USA

<sup>2</sup>Department of Physics and Astronomy and Bhaumik Institute for Theoretical Physics, University of California, Los Angeles, California 90095, USA

Note: This paper is part of the APL Special Collection on Topological and Chiral Matter—Physics and Applications.

<sup>a)</sup>Author to whom correspondence should be addressed: dp7bx@virginia.edu

#### **ABSTRACT**

We consider magnetic Weyl metals as a platform to achieve current control of magnetization textures with transport currents utilizing their underlying band geometry. We show that the transport current in a Weyl semimetal produces an axial magnetization due to orbital magnetic moments of the Weyl electrons. The associated axial magnetization can generate a torque acting on the localized magnetic moments. For the case of a magnetic vortex in a nanodisk of Weyl materials, this current-induced torque can be used to reverse its circulation and polarity. We discuss the axial magnetization torques in Weyl metals on general symmetry grounds and compare their strength to current-induced torques in more conventional materials.

Published under an exclusive license by AIP Publishing. https://doi.org/10.1063/5.0202451

Discrete degrees of freedom in condensed matter systems have firmly established themselves as perpetual candidates for information storage units. Their microscopic versions—single spins, single charges in single-electron boxes—have a long history of being considered for qubit realizations. Discrete macroscopic degrees of freedom, predominantly those associated with magnetization and its direction, have been not merely candidates but also workhorses of information storage, albeit classical one, see Refs. 1 and 2. Proposals to use mesoscopic magnetization textures in nanoscale samples as platforms for quantum information storage and manipulation have also emerged.3

Associated with these proposals is the question of control of small-scale magnetization textures. Accomplishing this control with electric currents promises practical benefits coming from scalability of the architectures and reduced power consumption, see Ref. 10 for a recent review of the field. In the realm of spintronics of conventional materials, 11 contrary to topological ones, there are a number of wellknown ways to approach magnetization control with current. The list includes spin-transfer torques in spin-valve-type devices, <sup>12</sup> spin current injection via spin Hall effect, 13 and current-induced torques in noncentrosymmetric systems with strong spin-orbit coupling.

In this work, we consider magnetic Weyl metals as a possible material candidate for realization of information storage and manipulation in nanoscale systems. We show that there is a source of current-induced spin torques in these materials related to the current-induced axial

We view a magnetic Weyl metal in the spirit of the s - d exchange model, which includes a subsystem of localized electrons responsible for the magnetization, and a system of itinerant electrons carrying transport currents. Our goal is to find a way to control the magnetization of localized electrons with the transport currents.

We use the prototypical model of a magnetic Weyl metal with only two Weyl points with opposite chiralities close to the Fermi level. Such a model preserves the inversion symmetry, but the time-reversal symmetry is broken by the magnetization, M, of the localized electrons.

The Hamiltonian of the model is given by 15,16

$$H_{\rm w} = \int d^3r \psi^{\dagger}(\mathbf{r}) [v \tau_z \mathbf{\sigma} \cdot \mathbf{p} - J \tau_0 \mathbf{\sigma} \cdot \mathbf{m}] \psi(\mathbf{r}), \tag{1}$$

where  $\psi(\mathbf{r})$  are the field operators for electrons, Pauli matrices  $\tau_z$  and  $au_0$  act in the valley space, while  $oldsymbol{\sigma}$  is a vector of Pauli matrices acting in the space spanned by the Weyl bands. The unit matrix  $\tau_0$  will not be explicitly written from here on. Furthermore, in Eq. (1), v is the Fermi speed, J is the exchange energy constant between itinerant electrons and localized spins,  $m \equiv M/M_s$  is a unit vector in the direction of the localized magnetization. In what follows, we assume that  $\sigma$  describes

the actual spin. This simplification is permissible as long as the magnetization of the localized electrons affects positions of the Weyl points in the momentum space as in model (1). For definiteness, we will assume v>0, and denote the  $\tau_z=\pm$  valleys with the chirality index  $\chi=\pm$ .

As simple as it is, the model (1) might pertain to the case of EuCd<sub>2</sub>As<sub>2</sub>, either in a small external magnetic field, <sup>17</sup> or grown in the ferromagnetic phase, as well as K<sub>2</sub>Mn<sub>3</sub>(AsO<sub>4</sub>)<sub>3</sub>. <sup>18</sup> However, one should keep in mind recent evidence that EuCd<sub>2</sub>As<sub>2</sub> is in fact a narrow-gap semiconductor. <sup>19</sup>

In this work, we will consider a Weyl magnet in which there exist both a static magnetic texture, m=m(r), and transport current density,  $j_{\rm tr}(r)$ . Our aim is to find a way to manipulate the texture with the transport current. A general way to achieve this goal follows from Eq. (1), which shows that the magnetization of the localized electrons couples to the spin polarization of the itinerant ones, which induces an effective Zeeman field,

$$\boldsymbol{B}_{\text{eff}} = \frac{J}{M_s} \langle \psi^{\dagger} \boldsymbol{\sigma} \psi \rangle, \tag{2}$$

where the  $\langle \ldots \rangle$  denotes the average with respect to the density matrix of the itinerant electrons, and  $M_s$  is the saturation magnetization of the localized electrons. In turn, the spin polarization of the itinerant electrons is identical to the axial current,  $j_5$ , defined as the difference in the individual valley currents,

$$\langle \psi^{\dagger} \sigma \psi \rangle = \frac{1}{ev} (j_{+} - j_{-}) \equiv \frac{1}{ev} j_{5},$$
 (3)

where  $\mathbf{j}_{\chi}$  is the current in the valley with chirality  $\chi$ , and e < 0 is the charge of the electron. The conclusion is that one must search for valley-asymmetric currents to control magnetization, or magnetic textures.

We argue that axial currents flow near sample boundaries when there is a current-induced axial magnetization. It can be induced in centrosymmetric samples with transport current. To describe this situation, we write down the expression for the magnetization in each valley as

$$\mathbf{M}_{\chi} = \int_{\mathbf{p}} \mu_{\chi,\mathbf{p}} f_{\chi,\mathbf{p}},\tag{4}$$

where  $\int_{\pmb{p}} \equiv \int \frac{d^3p}{(2\pi\hbar)^3}$ ,  $f_{\chi,p}$  is the occupation number of a state with quasimomentum  $\pmb{p}$  in valley  $\chi$  and in the band (conduction or valence) that contains a Fermi surface. We do not introduce the band index explicitly not to clutter the notation. Furthermore,  $\mu_{\chi,p}$  is the effective magnetic moment of an electron with quasimomentum  $\pmb{p}$ . Such a magnetic moment has both spin and orbital contributions, but the orbital effects are usually much stronger in Weyl materials, which is related to the fact that the Bohr magneton contains the bare electron mass, which is very large as compared to the effective mass scale,  $p_F/v$ , determining the orbital magnetic moments of Weyl electrons. (See note 28 in Ref. 20 for more details.)

It was shown in Ref. 21 that the orbital magnetic moments contain both an intrinsic contribution  $^{22}$  as well as extrinsic contributions from side jump and skew impurity scattering processes. However, for the simple isotropic model of Eq. (1), side jump and skew scattering processes vanish for isotropic impurity scattering, and only the intrinsic contribution needs to be taken into account. It would be enough to

add tilt to the dispersion of the Weyl cones to get an extrinsic contribution to the magnetic moment.<sup>23</sup>

For a single Weyl point of chirality  $\chi$ , we have the following expression for the intrinsic orbital angular moment:<sup>22</sup>

$$\mu_{\chi} = \chi \frac{e\hbar v}{2p} e_{p},\tag{5}$$

which works for both the conduction and valence bands, and where  $e_p$  is the unit vector in the direction of p. For definiteness, we assume that the Fermi level is in the conduction bands near the two Weyl points.

To calculate the axial magnetization of Weyl electrons, we use Eq. (4) with the nonequilibrium distribution function of the electrons in the presence of a transport electric field, E,  $\delta f_p = -\tau_{tr} e E \partial_p f_{eq}$ , with  $f_{eq}$  being the equilibrium Fermi–Dirac distribution in the band with the Fermi surface, and  $\tau_{tr}$  being the transport mean free time. Since both the transport current and the axial magnetization are determined by the same transport electric field, we can exclude it to obtain a direct relationship between the axial magnetization and the transport current,

$$M_5 \equiv M_+ - M_- = \frac{\hbar}{2p_F} \mathbf{j}_{\rm tr}.$$
 (6)

Using  $j_5 = \nabla \times M_5$  and combining Eq. (6) with Eqs. (2) and (3), we obtain the final expression for the current-induced effective Zeeman field in a centrosymmetric magnetic Weyl metal as follows:

$$\boldsymbol{B}_{\text{eff}} = \frac{\hbar J}{2e\epsilon_F M_s} \boldsymbol{\nabla} \times \boldsymbol{j}_{\text{tr}}, \tag{7}$$

where  $\epsilon_F \equiv p_F v$  is the Fermi energy counted from the energy of the Weyl nodes. To be valid, Eq. (7) requires that the model of Eq. (1), and the spin-momentum locking it implies, be applicable where  $\nabla \times j_{\rm tr} \neq 0$ . Herein, we assume that Eq. (1) applies all the way to the physical boundary of the sample, and that the magnetization of the localized electrons is finite at the edge, such that  $B_{\rm eff}$  can exert a torque on it. This remark makes it clear that in general the result for the torque will depend on the model of the sample edge.

Equation (7) for the effective Zeeman field is one of the central results of this work. Being determined by the curl of the transport current, this field vanishes in the bulk of an isotropic system, for which  $j_{\rm tr} = \sigma_D E$ , because of the Faraday's law for a static electric field,  $\nabla \times E = 0$ . For an anisotropic model, in which the conductivity is a nontrivial tensor, this field can exist even in the bulk of the system if the electric field is nonuniform. However, in any case, the effective field is nonzero near the boundary of a sample, if there is a flow of current along the boundary. Another important feature of Eq. (7) is that the magnitude of the effective field acting at the boundaries of a sample does not depend on the sample size as long as spatial quantization is not important.

We can gain further insight into the energy associated with the effective magnetic field,

$$E_{\text{eff}}^Z = - \int_{\mathbf{z}} \mathbf{B}_{\text{eff}} \cdot \mathbf{M}, \tag{8}$$

by relating it to the pseudomagnetic field induced by a magnetic texture. The pseudomagnetic field appears because in Hamiltonian (1), magnetization couples to the electrons in the two valleys as an axial

vector potential, having the opposite signs in the opposite valleys,  $eA_5 = \frac{\bar{I}}{v}m$ . Then it is clear that in the presence of a spatially varying magnetization, the axial vector potential  $A_5$  can develop a non-zero curl, and the corresponding pseudomagnetic field is

$$e\mathbf{B}_{5} = \frac{J}{v}\mathbf{\nabla} \times \mathbf{m},\tag{9}$$

see Refs. 24 and 25 for a review. If we now perform an integration by parts in Eq. (8) over a volume bounded by a surface outside the sample, over which the magnetization vanishes, we then trivially obtain

$$E_{\text{eff}}^Z = -\int_{\mathbf{r}} \mathbf{B}_5 \cdot \mathbf{M}_5, \tag{10}$$

where the current-induced axial magnetization is given by Eq. (6). Hence, the energy that we obtained is nothing but the Zeeman energy of the two axial magnetizations in the corresponding axial magnetic field due to a magnetic texture.

Before switching to applications, we would like to give another form of  $E_{\rm eff}^Z$ , appropriate for a sample with curl of the transport current confined to its surface,

$$E_{\text{eff}}^{Z} = -\frac{\hbar J}{2e\epsilon_{F}} \oint_{c} \mathbf{m} \cdot \mathbf{j}_{\text{tr}} \times \mathbf{n}. \tag{11}$$

The surface integral in the last term, representing the effective Zeeman energy, runs over the entire sample surface, and  $\boldsymbol{n}$  is the outer normal to the surface element dS. Expression (11) shows that the effective field (7) is not unique in its form: an analogous contribution would come from the spin Hall effect, see the discussion at the end of this paper. Our point is that this field in Weyl metals is strong enough to control magnetic textures even without a spin Hall effect. Conversely, if the spin Hall effect is being studied in a magnetic Weyl material, it should be kept in mind that the current-induced axial magnetization can affect interpretation of experiments.

The maximum effective field is determined by the maximum transport current. In a Weyl system, the maximum current in the linear regime is limited by the condition that the drift speed be smaller than the Fermi speed of Weyl electrons. In other words, the current is limited by  $j_{\rm max} = en_W v$ , where  $n_W$  is the total density of the Weyl electrons. Then from Eq. (7), it follows that the maximum effective field scales as  $B_{\rm eff}^{\rm max} \propto \epsilon_F^2$ , and saturates at  $\epsilon_F \sim J$ , where the Fermi surfaces near the two nodes go through a Lifshitz transition into a single trivial Fermi surface.

We now show that the current-induced effective Zeeman field is also effective in the sense of magnetization control. We consider a thin metallic disk shown in Fig. 1, in which a transport current is set up perpendicular to the plane of the disk. This current setup differs from the one considered for magnetic texture control in Ref. 16, where the current flow was in the plane of the disk. We assume that the transport current is reasonably uniform in the bulk of the disk and is mostly perpendicular to the top and bottom surfaces of the disk. In this case, the effective Zeeman field acts on the side surface of the disk, see Eq. (11) and Fig. 1. As is seen from Eq. (11), for Jv > 0, the field obeys the left hand rule, opposite to the Oersted field created by the current, because e < 0. We will neglect the Ørsted field for the time being, but later will show that for disks of sizes measured in tens of nanometers the effect of the Ørsted field is small as compared to the effective field considered in this paper.

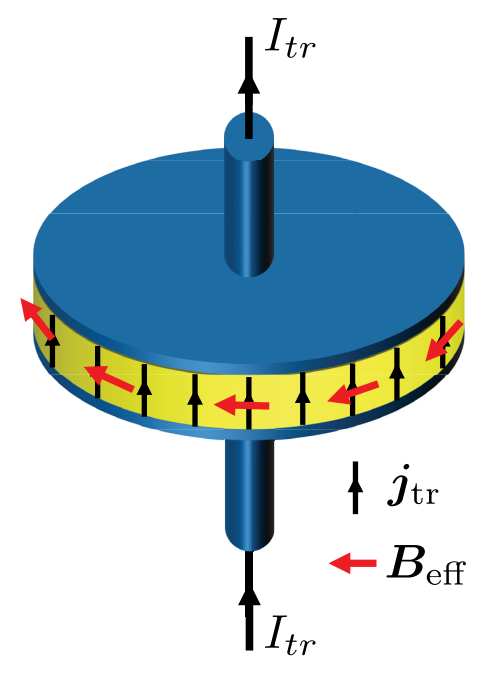


**FIG. 1.** Schematic drawing of a magnetic nanodisk (thick yellow disk) with two leads (thin dark blue disks) that feed in transport current  $l_{\rm tr}$ . The upward black arrows show the direction of transport current inside the disk, and the thick red arrows winding around the disk boundary represent the effective magnetic field induced by the current

Given the setup described earlier, it is clear that the effective Zeeman field gives preference to certain chirality of magnetic vortices and can switch between different chiralities for strong enough transport currents. Herein, we describe this process quantitatively.

We will assume that the magnetic energy of the disk,  $E_M$ , contains an exchange part associated with magnetization gradients, a dipolar part defined by the demagnetization field  $H_d$ , and the effective Zeeman part, Eq. (8), in the presence of a current,

$$E_{M} = A \int_{r} \nabla_{a} \boldsymbol{m} \nabla_{a} \boldsymbol{m} - \frac{\mu_{0} M_{s}}{2} \int_{r} \boldsymbol{m} \cdot \boldsymbol{H}_{d} + E_{\text{eff}}^{Z}.$$
 (12)

In the absence of proven materials known to realize a simple magnetic Weyl metal model (1), we will use the typical values of magnetic quantities for estimates:  $A=10^{-11}\,\mathrm{J/m}$  for the exchange constant,  $\mu_0 M_s=1\,\mathrm{T}$  for the saturation magnetization, and  $J/\epsilon_F\sim 10$  in the expression for the effective Zeeman energy, Eq. (11). Additional discussion on the effect of  $J/\epsilon_F$  is provided in Sec. I of the supplementary material. For these numbers, the magnetic exchange length is  $\ell_{\rm ex}=\sqrt{2A/\mu_0}M_s^2\approx 5\,\mathrm{nm}$ . We neglect the Ørsted field of the current, as its effect is small for the sizes of the disks considered, which we checked numerically.

A disk of large enough radius contains a magnetic vortex<sup>26</sup> of the in-plane magnetization, see Fig. 2. The vortex develops to minimize the dipolar energy at the expense of an increase in the exchange

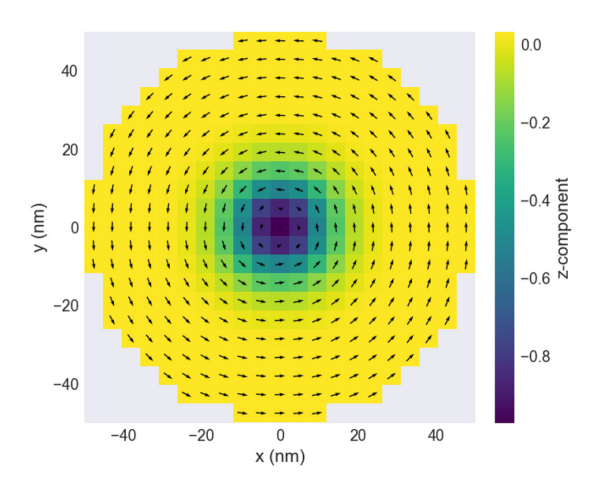


**FIG. 2.** Magnetic vortex configuration in a disk of thickness 25 nm and radius 50 nm. The polarity of the vortex is -1 (topological charge  $-\frac{1}{2}$ ), and its chirality is +1.

energy. To keep the exchange energy finite, a vortex must have a core with out-of-plane magnetization. Then a vortex is characterized with two discrete indices, each taking values  $\pm 1$ : the chirality of magnetization winding away from the core and the polarization direction of the core. The four possible combinations of these indices are all degenerated for the energy (12) in the absence of a transport current.

It is worth noting that magnetic vortices of the described kind have definite positive winding for either sign of the chirality, in the sense that the azimuthal angle of the magnetization,  $\phi$ , winds in the positive direction with the azimuthal angle of the cylindrical coordinate system in real space,  $\theta$ , the z-axis of which goes through the center of the disk, perpendicular to its plane,

$$\phi = \theta + \pi/2 + \eta. \tag{13}$$

In the equation for the azimuthal angle of the magnetization, the quantity  $\eta=0,\pi$  correspond to positive and negative chirality, respectively. An anti-vortex with negative winding would create magnetization pattern with nonzero radial component at the disk side surface, and thus would have high magnetostatic energy due to the magnetic charges on that surface.

The fixed winding makes the topological index of the vortex, or its skyrmion charge,

$$N(z) = \frac{1}{4\pi} \int dx dy \, \mathbf{m}(\mathbf{r}) \cdot (\partial_x \mathbf{m}(\mathbf{r}) \times \partial_y \mathbf{m}(\mathbf{r})), \tag{14}$$

dependent on the vortex core polarization only. Since the sample is three-dimensional, one can only define the topological charge for z= const plane, and the result is z-dependent. However, we checked numerically that even for a disk of diameter only twice as large as its thickness, the skyrmion charge N(z) as a function of z does not deviate from the values of  $\pm 1/2$  by more than 5%, so we are dealing with well-defined vortices.

We define the chirality as the volume integral over the interior of the sample, not including its boundary, of the z-component of the magnetization direction curl,

$$C = \frac{1}{2\pi r d} \int d^3 r \, \boldsymbol{e}_z \cdot \nabla \times \boldsymbol{m}. \tag{15}$$

This expression saturates at  $\pm 1$  for a vortex with the magnetization direction, m, independent of the z-coordinate, and lying in the xy-plane near the sample boundary. For small and thin disks, these conditions are satisfied with high accuracy.

Without a current, the two vortex chiralities are degenerate in energy. This is inferred from the chirality definition (15) and Eq. (10) for the effective Zeeman energy expressed via current-induced axial magnetization and Eq. (6) for the axial magnetization itself. As a result, for a transport current along the disk axis, the effective Zeeman energy is proportional to the average disk chirality. Hence, it makes one of the chirality states metastable. The Ørsted field of the current would have the same qualitative effect, but for disk diameters around hundred nanometers the effect of the Ørsted field is small. For large enough current, the metastability is removed, and the effective field induces deterministic switching into the low-energy state. We now proceed with a numerical analysis of the switching current.

To obtain the critical current for the chirality switching, we simulated the system dynamics with slowly varying values of the transport current to determine the value at which the chirality switches. Additional graphs of the temporal dependence of the vortex chirality and of the magnetic texture evolution are shown in the supplementary material, Figs. S1–S3. The results of the simulation for a disk of radius 50 nm and variable thickness are shown in Fig. 3. We obtained critical currents of the order of  $5 \times 10^{11} \, \text{A/m}^2$ , which are feasible from the practical point of view. Equating the value of the critical current to the maximum achievable current in the linear regime,  $j_{\text{max}} = e n_W v$ , and using  $v = 10^5 \, \text{m/s}$ , we see that the required carrier density is  $n_W \sim 10^{19} \, \text{cm}^{-3}$ . Hole doping of  $10^{20} \, \text{cm}^{-3}$  in EuCd<sub>2</sub>As<sub>2</sub> was reported in Ref. 27.

We also noticed empirically that for relatively large values of the Gilbert damping constant, the polarization of the core switched together with the chirality in small disks. The typical graphs of the chirality and the skyrmion number as functions of the applied static current are shown in Fig. 4. Note that with decreasing value of  $\alpha_G$ , the

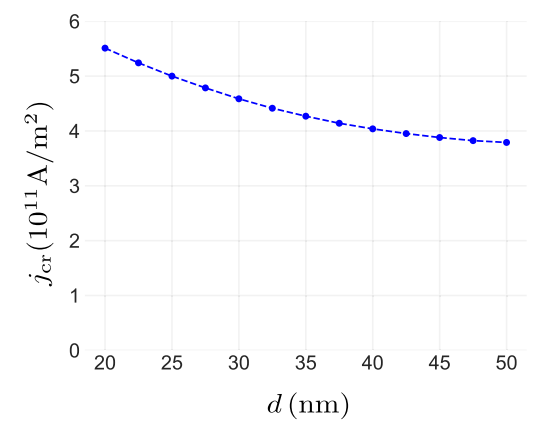


**FIG. 3.** Critical switching current,  $j_{\rm cr}$ , for a disk of 50 nm radius as a function of its thickness. d.

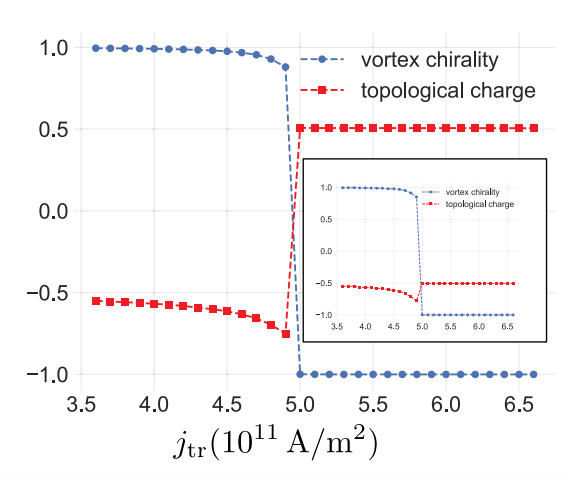


**FIG. 4.** Chirality of a magnetic vortex and its topological charge as a function of transport current density,  $j_{\rm tr}$ , as it is gradually increased. Both the main panel and the inset correspond to numerical simulations of the Landau–Lifshitz–Gilbert equation for a disk sample with a thickness of 25 nm and a radius of 50 nm. In the main panel, the Gilbert damping constant is  $\alpha_{\rm G}=0.01$ , while, in the inset,  $\alpha_{\rm G}=0.001$ . The small value of  $\alpha_{\rm G}$  did not lead to polarization reversal, while the critical current for chirality reversal remained the same.

polarization fails to switch, while the critical current does not change. This shows that the polarization switching is a dynamic effect, which is sensitive to the speed of the chirality reversal, while the chirality itself switches when it loses metastability, regardless of how fast the subsequent dynamics is.

Finally, we note that for pure Ørsted field of the current, neglecting the effective boundary field, the critical switching current for the geometry considered here is roughly  $5\times 10^{12}\,\mathrm{A/m^2}$ , and order of magnitude larger than for the boundary field. This is consistent with the findings of Ref. 28, and shows that neglecting this field was justified for our purposes. Of course, for large enough disks, the Ørsted field will eventually dominate the switching.

It is interesting to compare this mechanism with proposals to generate axial currents, and hence itinerant spin polarization, in current-carrying Weyl metals in the existing literature. In Ref. 16, it was shown that axial Hall effect, driven by the pseudomagnetic field  $\emph{\textbf{B}}_{5}$ , drives an axial Hall current  $\emph{\textbf{j}}_{5} \propto \emph{\textbf{B}}_{5} \times \emph{\textbf{j}}_{tr}$ . Later in Ref. 29, the axial version of the chiral magnetic effect was used in conjunction with the chiral anomaly to generate  $j_5 \propto B_5(B \cdot j_{tr})$ , where B is the external (but which can be the field of the magnetization itself) magnetic field driving the chiral anomaly. In contrast, in this work, the axial current takes the form of  $j_5 \propto \nabla \times j_{tr}$ . This axial current, unlike those from Refs. 16 and 29, is not proportional to  $B_5$ , Eq. (9). This makes it at least one or maybe two orders of magnitude smaller than the other two axial currents, since  $B_5$  is large due to the large value of the exchange constant and small exchange length that determines the size of magnetic textures in ferromagnets. However, its independence from  $B_5$  is also its strength from the symmetry point of view: the axial current considered here is even in the localized magnetization, and hence can distinguish chiralities of a magnetic vortex. As we demonstrated, the magnitude of the effect is sufficient to drive chirality reversals in

nanosized samples more efficiently than with the Ørsted field of the current. Further discussion of relevant physical phenomena is presented in Sec. I of the supplementary material.

It is also interesting to compare the boundary spin polarization associated with the axial magnetization current to the one that would have been induced by an isotropic spin Hall effect, if it existed in the sample. In that case, the spin polarization current is given by  $j_b^a = \theta \epsilon_{abc} j_{{
m tr},c}/e$ , where  $j_b^a$  is the current of ath component of spin polarization in the bth spatial direction, and  $\theta$  is the spin Hall angle. Then for electric current flowing in the z-direction along the boundary perpendicular to the x-direction, there is a spin accumulation of surface density of the yth component of spin polarization of magnitude  $\sim \tau_{\rm sf} \theta j_{\rm tr}/e$ . This result needs to be compared to the spin accumulation given by the current-induced axial magnetization current, given by  $\sim \hbar j_{\rm tr}/e\epsilon_F$ . For instance, for Pt  $\tau_{\rm sf} \sim 10^{-14}$  s,  $^{30}$  and  $\theta \sim 10^{-1}$ ,  $^{31}$  which yields  $\tau_{sf} \theta \sim 10^{-15}$  s. For the mechanism described in this work and the typical  $\epsilon_F \sim 50$  meV, we obtain  $\hbar/\epsilon_F \sim 10^{-14}$  s, obviously implying a much larger boundary spin polarization. This order of magnitude larger boundary spin polarization may even be utilized in the spintronics applications.

See the supplementary material for a general discussion of physical phenomena in current-carrying Weyl metals with magnetic textures and illustrations of time dependence of vortex chirality switching.

The work of J.-G.Y. and D.A.P. was supported by the National Science Foundation under Grant No. DMR-2138008. The work of Y.T. was supported by the U.S. Department of Energy, Office of Basic Energy Sciences, under Award No. DE-SC0012190.

## AUTHOR DECLARATIONS Conflict of Interest

The authors have no conflicts to disclose.

#### **Author Contributions**

J.-G. Yang: Formal analysis (equal); Investigation (equal); Writing – original draft (equal); Writing – review & editing (equal). Y. Tserkovnyak: Conceptualization (equal); Investigation (equal); Writing – original draft (equal); Writing – review & editing (equal). D. A. Pesin: Conceptualization (equal); Formal analysis (equal); Funding acquisition (lead); Project administration (lead); Supervision (equal); Writing – original draft (equal); Writing – review & editing (equal).

#### DATA AVAILABILITY

Data sharing is not applicable to this article as no new data were created or analyzed in this study.

#### REFERENCES

- <sup>1</sup>S. S. Parkin, M. Hayashi, and L. Thomas, Science 320, 190 (2008).
- <sup>2</sup>G. Tatara, H. Kohno, and J. Shibata, Phys. Rep. 468, 213 (2008).
- <sup>5</sup>H.-B. Braun and D. Loss, J. Appl. Phys. **76**, 6177 (1994). <sup>4</sup>S. Takagi and G. Tatara, Phys. Rev. B **54**, 9920 (1996).
- <sup>5</sup>L. Caretta, M. Mann, F. Büttner, K. Ueda, B. Pfau, C. M. Günther, P. Hessing,
- A. Churikova, C. Klose, M. Schneider *et al.*, Nat. Nanotechnol. **13**, 1154 (2018).

- <sup>6</sup>C. Psaroudaki and C. Panagopoulos, Phys. Rev. Lett. 127, 067201 (2021).
  <sup>7</sup>L. J. Heyderman, J. Grollier, C. H. Marrows, P. Vavassori, D. Grundler, D. Makarov, and S. Pané, Appl. Phys. Lett. 119(8), 080401 (2021).
  <sup>8</sup>J. Xia, X. Zhang, X. Liu, Y. Zhou, and M. Ezawa, Commun. Mater. 3, 88 (2022).
- <sup>9</sup>R. Jangid, N. Z. Hagström, M. Madhavi, K. Rockwell, J. M. Shaw, J. A. Brock, M. Pancaldi, D. De Angelis, F. Capotondi, E. Pedersoli et al., Phys. Rev. Lett. 131, 256702 (2023).
- <sup>10</sup>A. Fert, R. Ramesh, V. Garcia, F. Casanova, and M. Bibes, arXiv:2311.11724
- <sup>11</sup>I. Žutić, J. Fabian, and S. D. Sarma, Rev. Mod. Phys. 76, 323 (2004).
- <sup>12</sup>D. C. Ralph and M. D. Stiles, J. Magn. Magn. Mater. 320, 1190 (2008).
- <sup>13</sup>J. Sinova, S. O. Valenzuela, J. Wunderlich, C. H. Back, and T. Jungwirth, Rev. Mod. Phys. 87, 1213 (2015).
- <sup>14</sup>A. Manchon, J. Železný, I. M. Miron, T. Jungwirth, J. Sinova, A. Thiaville, K. Garello, and P. Gambardella, Rev. Mod. Phys. 91, 035004 (2019).
- 15 N. Armitage, E. Mele, and A. Vishwanath, Rev. Mod. Phys. 90, 015001 (2018). <sup>16</sup>D. Kurebayashi and K. Nomura, Sci. Rep. **9**, 5365 (2019).
- <sup>17</sup>J.-R. Soh, F. de Juan, M. G. Vergniory, N. B. M. Schröter, M. C. Rahn, D. Y. Yan, J. Jiang, M. Bristow, P. Reiss, J. N. Blandy et al., Phys. Rev. B 100, 201102 (2019). <sup>18</sup>S. Nie, T. Hashimoto, and F. B. Prinz, Phys. Rev. Lett. **128**, 176401 (2022).

- 19 D. Santos-Cottin, I. Mohelský, J. Wyzula, F. Le Mardelé, I. Kapon, S. Nasrallah, N. Barišić, I. Živković, J. R. Soh, F. Guo et al., Phys. Rev. Lett. 131, 186704 (2023).

  20 J. Ma and D. A. Pesin, Phys. Rev. B **92**, 235205 (2015).
- J. Rou, C. Şahin, J. Ma, and D. A. Pesin, Phys. Rev. B 96, 035120 (2017).
   D. Xiao, M.-C. Chang, and Q. Niu, Rev. Mod. Phys. 82, 1959 (2010).
- <sup>23</sup>J. F. Steiner, A. V. Andreev, and D. A. Pesin, Phys. Rev. Lett. 119, 036601 (2017).
- <sup>24</sup>Y. Araki, Ann. Phys. **532**, 1900287 (2020).
- <sup>25</sup>R. Ilan, A. G. Grushin, and D. I. Pikulin, Nat. Rev. Phys. **2**, 29 (2019).
- <sup>26</sup>W. F. Brown, *Micromagnetics* (Wiley, New York, 1963).
- <sup>27</sup>S. Roychowdhury, M. Yao, K. Samanta, S. Bae, D. Chen, S. Ju, A. Raghavan, N. Kumar, P. Constantinou, S. N. Guin et al., Adv. Sci. 10, 2207121 (2023).
- <sup>28</sup>W. A. S. Aldulaimi, M. B. Okatan, K. Sendur, M. Onbasli, and I. Misirlioglu, cale 15, 707 (2023).
- <sup>29</sup>J. Hannukainen, A. Cortijo, J. H. Bardarson, and Y. Ferreiros, SciPost Phys. 10, 102 (2021).
- <sup>30</sup>R. Freeman, A. Zholud, Z. Dun, H. Zhou, and S. Urazhdin, Phys. Rev. Lett. 120, 067204 (2018).
- <sup>31</sup>W. Zhang, V. Vlaminck, J. E. Pearson, R. Divan, S. D. Bader, and A. Hoffmann, Appl. Phys. Lett. 103(24), 242414 (2013).